CHAPTER IV
RESULTS AND DISCUSSION

4.1 Rheological Characterizations

4.1.1 Molecular Weight Characterization

The molecular weights (M_w and M_n) and molecular weight dispersities (MWD) of PP and PS characterized by the cone and plate rheometer are shown in Table 4.1. The weight average molecular weights of PP are close to the values quoted from company (Table 3.1). But the molecular weights of PS are not available from the company.

Table 4.1 The molecular weights and molecular weight dispersities of PP and PS as characterized by the rheological method

Polymers	Molecular Weights		Polydispersity
	M_w	M_n	(M_w/M_n)
PP (1)	7.98×10^6	3.41×10^5	23.40
	($\pm 1.15 \times 10^6$)	($\pm 0.01 \times 10^5$)	(±3.42)
PP (2)	7.09×10^6	3.32×10^5	21.45
	($\pm 0.58 \times 10^6$)	($\pm 0.25 \times 10^5$)	(±3.41)
PP (3)	6.19×10^6	2.62×10^5	24.39
	($\pm 0.14 \times 10^6$)	($\pm 0.66 \times 10^5$)	(±5.64)
PP (4)	4.45×10^6	2.15×10^5	20.73
	($\pm 0.19 \times 10^6$)	($\pm 0.09 \times 10^5$)	(±0.02)
PS (1)	2.62×10^5	1.23×10^5	2.18
	($\pm 0.38 \times 10^5$)	($\pm 0.38 \times 10^5$)	(±0.35)
PS (2)	1.69×10^5	4.27×10^4	4.24
	($\pm 0.21 \times 10^5$)	($\pm 0.19 \times 10^4$)	(±1.35)
PS (3)	8.05×10^4	2.72×10^3	2.96
	($\pm 0.50 \times 10^5$)	($\pm 0.01 \times 10^3$)	(±1.73)

4.1.2 Shear Viscosity (η)

The shear viscosities of homopolymers PP and PS as a function of shear strain rate at 220 ^{0}C are shown in Figures 4.1 (a) and 4.1 (b). Each measurement of shear viscosity as a function of shear strain rate was repeated over 4-6 times, and average values are reported. All of the homopolymers show the shear-thinning characteristic. At sufficiently low shear strain rates, the shear viscosities of PS(2), PS(3), and PP(4) show Newtonian plateaus; the shear viscosity does not vary with the shear strain rate. PS(1), PP(1), PP(2), and PP(3) do not show this behavior. The shear viscosity, obtained by extrapolating the Newtonian plateaus to zero shear strain rate is called zero shear viscosity and denoted as η_0. In many studies reported, η_0 is proportional to the molecular weight with the power-law scaling exponent of 3.4 if M_w is above the entanglement molecular weight (Dealy and Wissbrun, 1990). The zero shear viscosities from the homopolymers used are tabulated in Table 4.2.

Table 4.2 The zero shear viscosities of all homopolymers at 220 ^{0}C

Polymers	Zero shear viscosity (Poise)
PP(1)	$9.36 \pm 0.87 \times 10^4$
PP(2)	$6.32 \pm 0.36 \times 10^4$
PP(3)	$4.44 \pm 0.02 \times 10^4$
PP(4)	$1.76 \pm 0.13 \times 10^4$
PS(1)	$1.27 \pm 0.04 \times 10^5$
PS(2)	$1.50 \pm 0.16 \times 10^4$
PS(3)	$9.14 \pm 0.47 \times 10^3$

The results from the zero shear viscosity measurement are consistent with the results from the molecular weight measurement. PS(1), the highest molecular weight, has the highest value of the zero shear viscosity whereas PS(3), the lowest molecular weight, has the lowest value of zero shear viscosity.

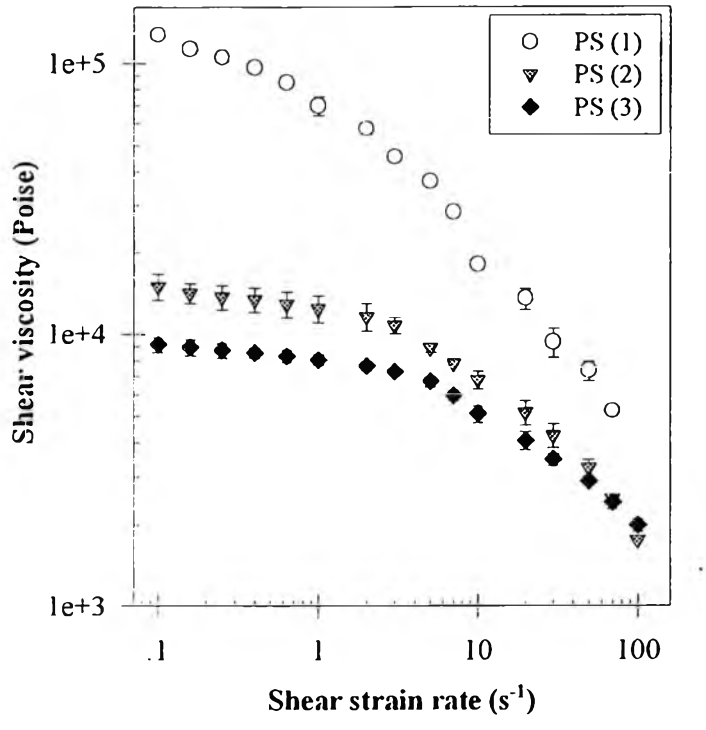

Figure 4.1 (a) The shear viscosities of PS (1), PS (2), and PS (3) as a function of shear strain rate at 220 ^{0}C.

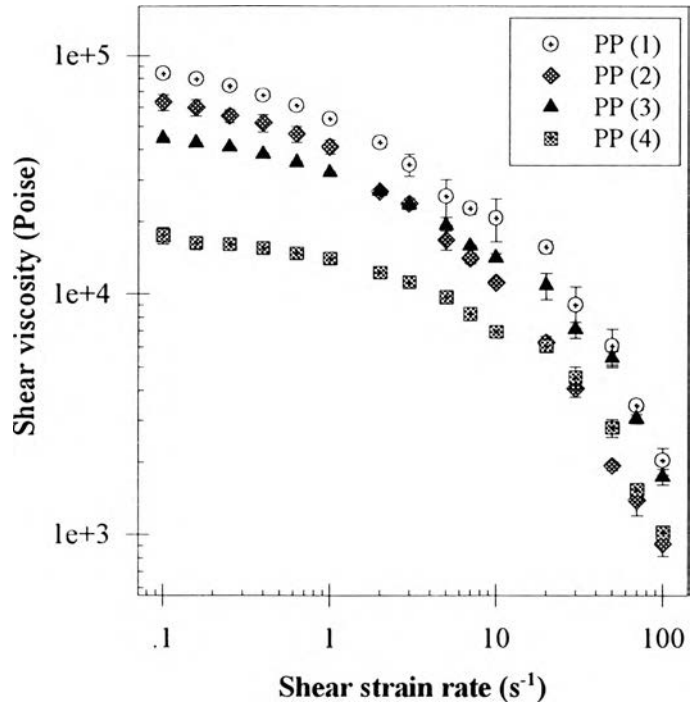

Figure 4.1 (b) The shear viscosities of PP (1), PP (2), PP (3), and PP (4) as a function of shear strain rate at 220 ^{0}C.

4.1.3 The First Normal Stress Difference (N_1)

The first normal stress difference of homopolymers PP and PS as a function of shear strain rate at 220 ^{0}C are shown in Figures 4.2(a) and 4.2(b). Each N_1 measurement as a function of shear strain rate was repeated over 4-5 times, and average values are reported. The first normal stress difference of polymer melt usually has a power-law behavior over range of shear strain rates, and can be written as

$$N_1 = A(\dot{\gamma}^m) \qquad (4.1)$$

where A and m are constant, with m being typically in the range $1 < m \leq 2$ (Barnes *et al.*, 1989). All homopolymers from this experiment show positive N_1 values and the power-law behavior of N_1 with the power law exponent of 1. A higher molecular weight homopolymer shows a higher N_1. At high shear strain rates, N_1 of PS and PP shows some bending from the power-law behavior due to the transducer limitation of 1 x 10^6 dyn/cm^2.

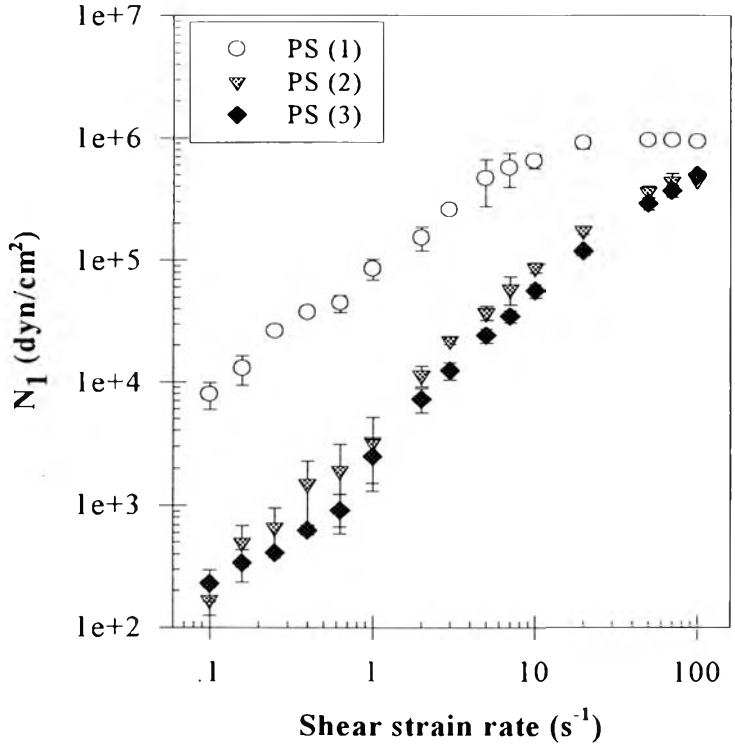

Figure 4.2 (a) The first normal stress difference of PS (1), PS (2), and PS (3) as a function of shear strain rate at 220 ^{0}C.

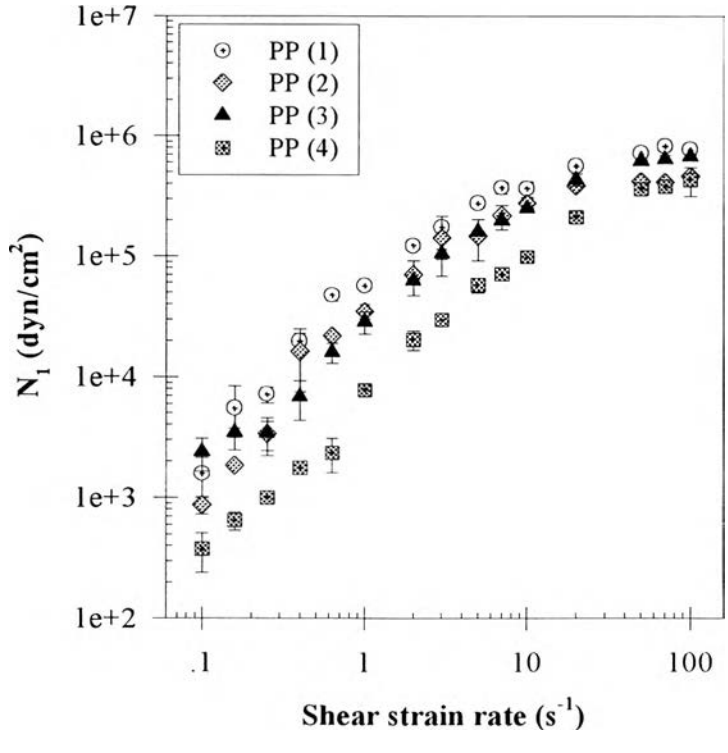

Figure 4.2 (b) The first normal stress difference of PP (1), PP (2), PP (3), and PP (4) as a function of shear strain rate at 220 ^{0}C.

4.1.4 Polymer Degradation

After processing for a long time, the rheological properties of polypropylenes were found to change gradually, due to polymer degradation. The mechanism of PP degradation is shown in Figure 4.3 (Schnabel, 1981). From Figure 4.3, the tertiary carbon (a), the most reactive carbon on backbone can be attacked by O_2 in the air to form peroxide (b). Due to the instability of peroxide, hydroxide radical is removed (c). Carbonyl and methylene radical (d) are formed leading to the chain scission. Therefore M_w is reduced after a long processing time. So the post processing characterization is necessary in determining some changes in rheological properties of the polypropylenes.

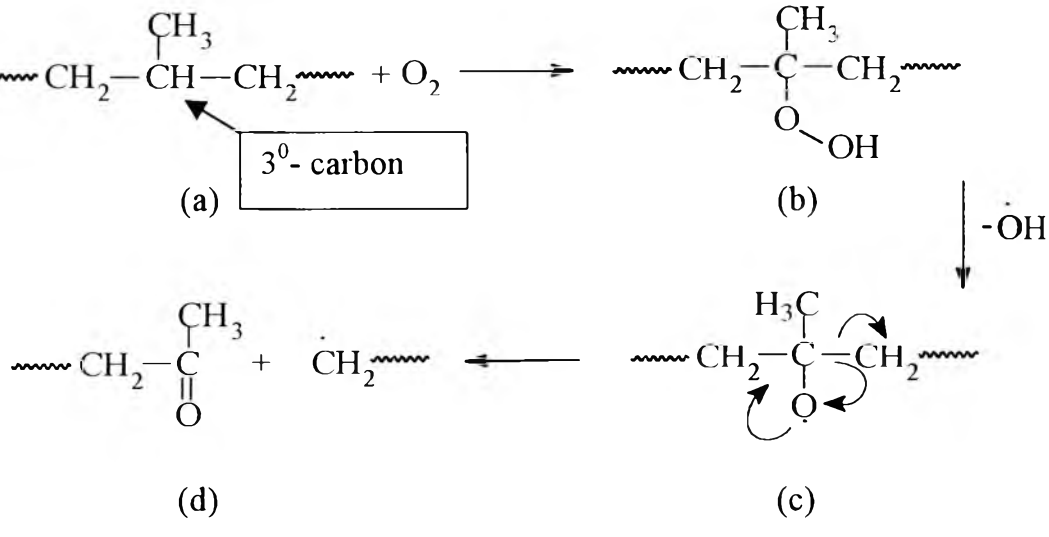

Figure 4.3 The degradation mechanism of Polypropylene in the presence of O_2.

The shear viscosities of the polypropylenes after processing for 300 s, 500 s and 1000 s are comparable to the initial value and plotted versus shear strain rate, at 220 ^{0}C, as presented in Figure 4.4 (a-d). The shear viscosities of the polypropylenes decrease with processing time implying that the degradation of polypropylene occurred.

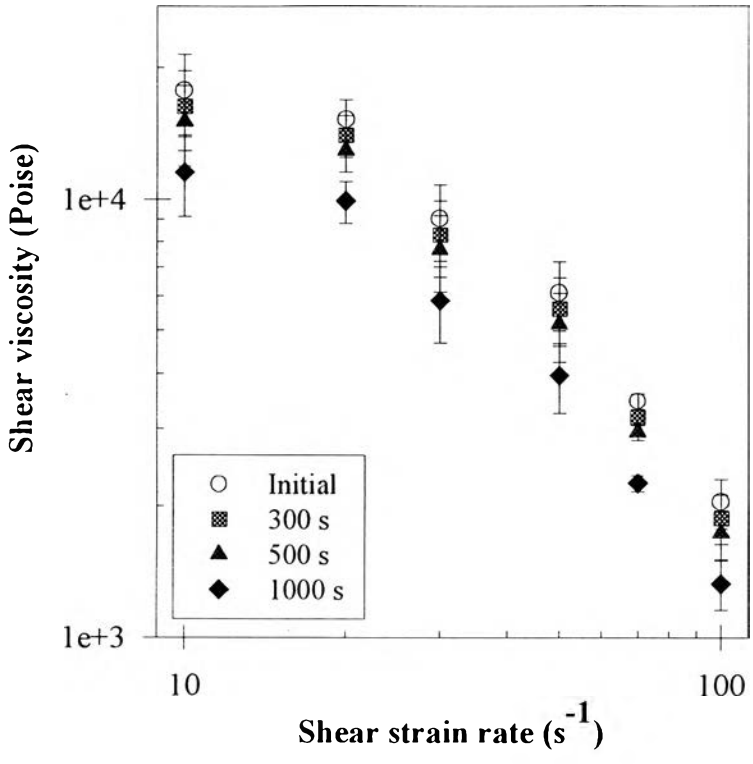
Shear viscosity (Poise)
1e+4
1e+3
Initial
300 s
500 s
1000 s
10
100
Shear strain rate (s-1)

(a)

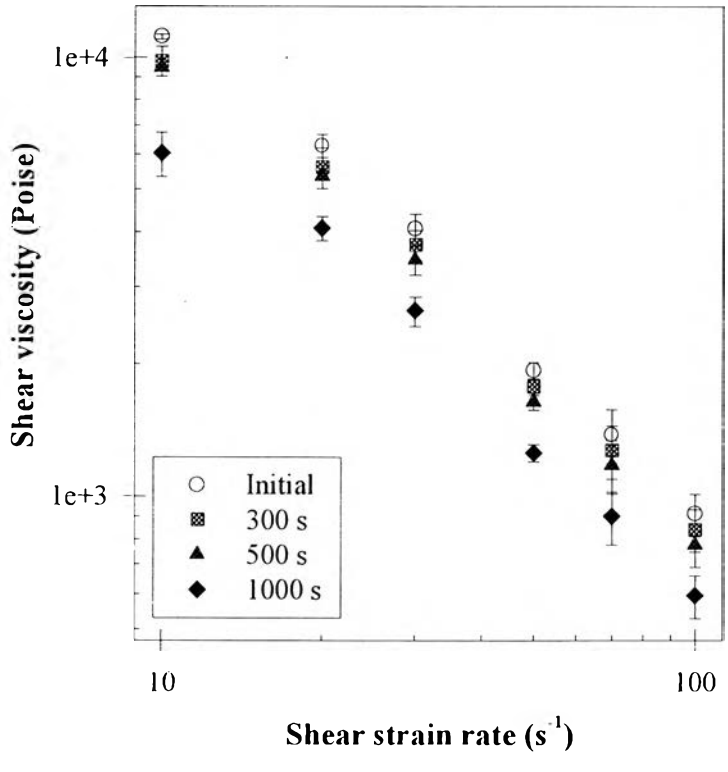
Shear viscosity (Poise)
1e+4
1e+3
Initial
300 s
500 s
1000 s
10
100
Shear strain rate (s-1)

(b)

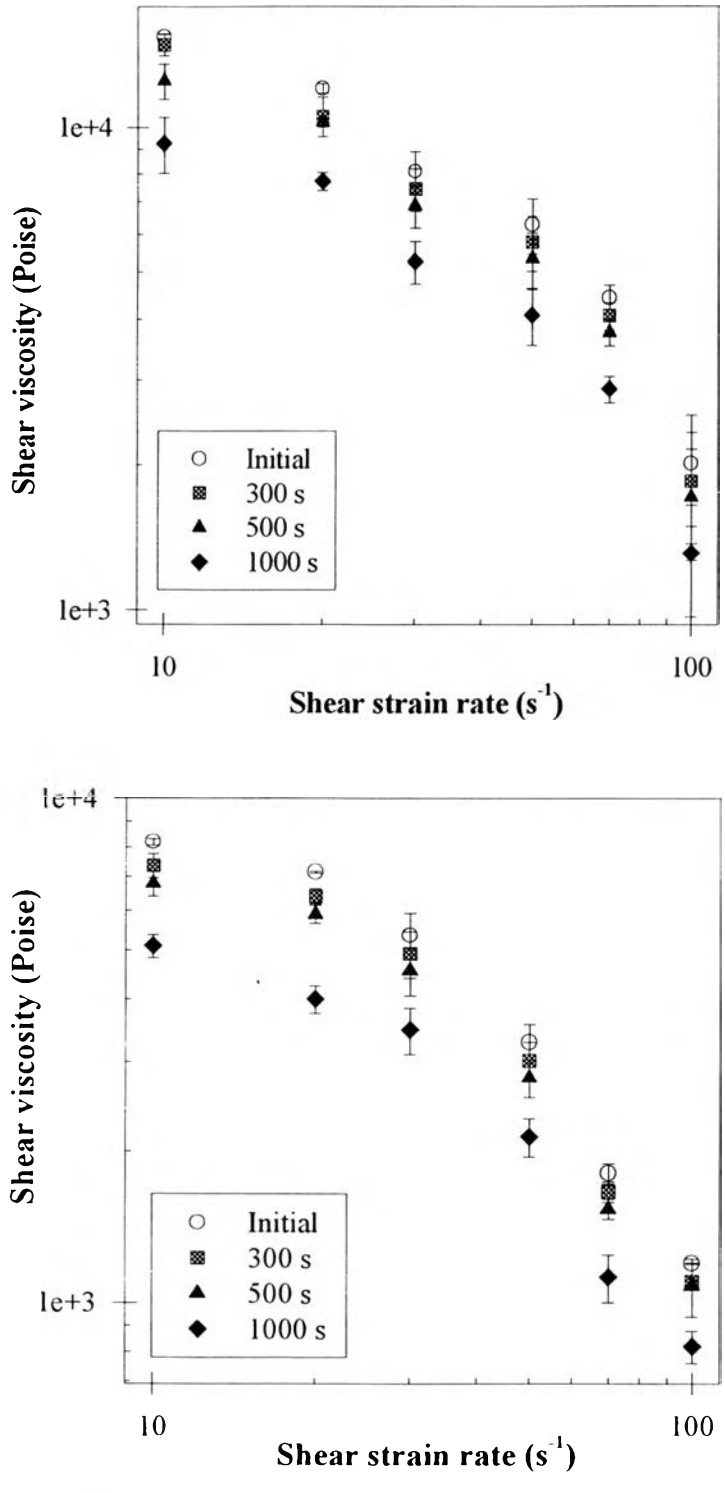

Figure 4.4 Pre processing and post processing shear viscosity of PP for 300 s, 500 s, and 1000 s as a function of shear strain rate at 220 ^{0}C: (a) PP(6631); (b) PP (pd382); (c) PP (6531); and (d) PP (pd943).

The final zero shear viscosities after shearing at 300 s, 500 s, and 1000 s are comparable to the initial zero shear viscosities and tabulated in Table 4.3. The zero shear viscosity of PP(1) changed from 9.37 x 10^4 g/mole to 8.59 x 10^4 g/mole (8.27 % change) after shearing for 300 s, from 9.37 x 10^4 g/mole to 7.92 x 10^4 g/mole (15.38 % change) after shearing for 500 s, and from 9.37 x 10^4 g/mole to 5.64 x 10^4 g/mole (39.75 % change) after shearing for 1000 s. These results indicate that the polymer degradation can be minimized by decreasing the processing time.

Table 4.3 The initial zero shear viscosity and the final zero shear viscosity of PP after shearing at 220 ^{0}C

Polymer	The zero shear viscosity (Poise)			
	Initial	300 s	500 s	1000 s
PP(1)	9.37 x 10^4 ($\pm$ 0.25 x 10^4)	8.59 x 10^4 $\pm$ 0.54 x 10^4	7.92 x 10^4 $\pm$ 0.22 x 10^4	5.64 x 10^4 $\pm$ 0.04 x 10^4
% change		8.27 ($\pm$ 2.56)	15.38 ($\pm$ 2.25)	39.75 ($\pm$ 0.35)
PP(2)	6.32 x 10^4 $\pm$ 0.48 x 10^4	5.82 x 10^4 $\pm$ 0.32 x 10^4	5.48 x 10^4 $\pm$ 0.42 x 10^4	3.96 x 10^4 $\pm$ 0.21 x 10^4
% change		7.82 ($\pm$ 2.84)	13.29 ($\pm$ 6.64)	37.29 ($\pm$ 3.29)
PP(3)	4.44 x 10^4 $\pm$ 0.02 x 10^4	4.10 x 10^4 $\pm$ 0.18 x 10^4	3.82 x 10^4 $\pm$ 0.13 x 10^4	2.88 x 10^4 $\pm$ 0.19 x 10^4
% change		7.61 ($\pm$ 3.60)	13.74 ($\pm$ 2.70)	34.92 ($\pm$ 4.02)
PP(4)	1.75 x 10^4 $\pm$ 0.13 x 10^4	1.58 x 10^4 $\pm$ 0.12 x 10^4	1.49 x 10^4 $\pm$ 0.21 x 10^4	1.10 x 10^4 $\pm$ 0.32 x 10^4
% change		9.35 ($\pm$ 2.85)	14.30 ($\pm$ 2.85)	36.61 ($\pm$ 1.89)

4.2 Effect of Shearing Time

4.2.1 Droplet Size

The number average diameters of PS(1) dispersed in PP(4) and PS(2) dispersed in PP(3) were plotted as a function of shear strain, the product of shearing time multiplied by shear strain rate at shear strain rates of 10 and 100 s^{-1} and are shown in Figure 4.5. Two blend systems have different viscosity ratios in the shear strain rate range between 10–100 s^{-1}. The viscosity ratio of PS(1)/PP(4) is around 3 and of PS(2)/PP(3) is around 0.5. The number average diameters of the PS(1)/PP(4) and PS(2)/PP(3) blends at the shear strain rates of 10 and 100 s^{-1} decrease with increasing shear strain unit, followed by the leveling off to plateau values when the shear strain unit reaches 5000, meaning that the ensemble mean droplet size has been attained an equilibrium at the shear strain around 5000. The results suggest that the morphology was developed rapidly in the initial stage of deformation (Bourry and Favis, 1998). The morphology obtained from shearing at shear strain units 5000 and 20000 do not differ even though rheological properties change significantly as reported in section 4.1.4. It can be concluded that the final rheological properties do not influence the equilibrium droplet size.

For a better understanding, the ensemble mean average diameters of dispersed phase over the equilibrium diameter were plotted versus the shear strain unit and are shown in Figure 4.6. This plot shows that the equilibrium droplet size of dispersed phase is obtained where the shear strain unit exceeds the value of 5000.

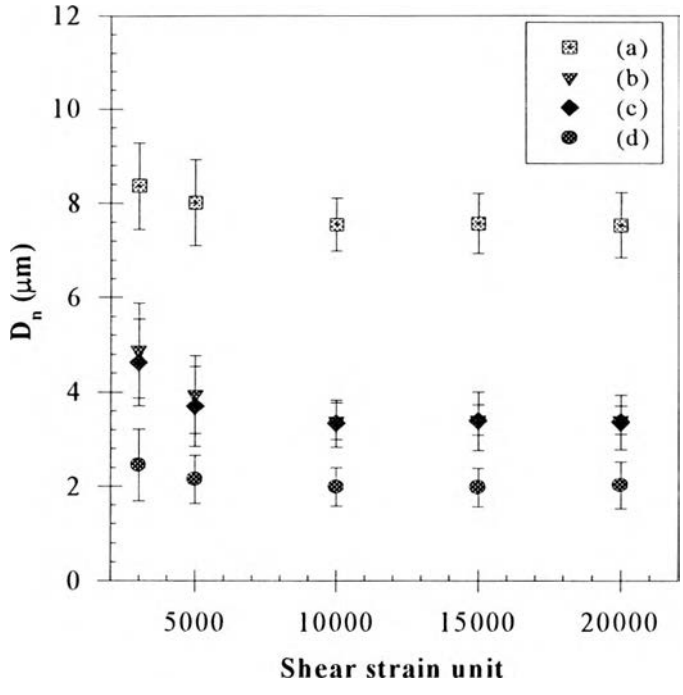

Figure 4.5 The number average diameter of dispersed phase PS versus shear strain unit at 220 ^{0}C; (a) PS(1)/PP(4) at γ =10 s^{-1}; (b) PS(1)/PP(4) at γ =100 s^{-1}; (c) PS(2)/PP(3) at γ =10 s^{-1}; (d) PS(2)/PP(3) at γ =100 s^{-1}.

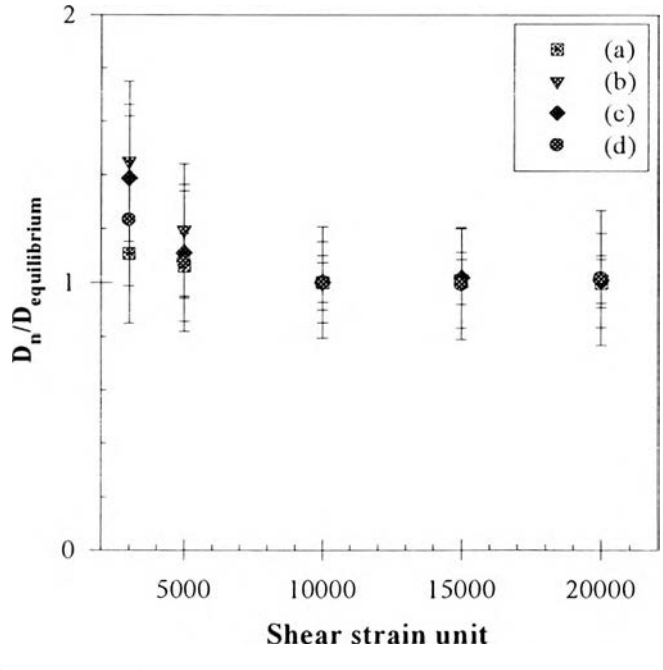

Figure 4.6 The plot of ($D_n/D_{equilibrium}$) versus shear strain unit of dispersed phase PS at 220 ^{0}C.

4.2.2 Distribution Function of Droplet Size

To investigate the morphology change with shear strain unit at any shear strain rates, the size distribution functions were measured and determined. The droplet size distributions of PS(1)/PP(4) and PS(2)/PP(3) as a function of shear strain unit at the shear strain rate of 10 and 100 s^{-1}, at 220 ^{0}C are shown in Figures 4.7 to 4.10, respectively. At the shear strain rates of 10 and 100 s^{-1}, the droplet size distribution changes with shear strain unit for both blend systems. At the shear strain unit 3000 and 5000, the bimodal distributions occur. When the shear strain unit reaches 10000, the distribution shows a narrow and monomodal distribution. The droplet size distributions for shear strain units of 15000 and 20000 are shown in Appendix C. The results suggest that the statistical distribution function changes slightly after a sufficient shearing time, consistent with the result of Scott *et al.* (1995).

The micrographs obtained from the optical microscope for the effect of shearing time are shown in Appendix B. The statistical data of droplet size at the shear strain rates of 10 and 100 $s^{-1}$of PS(1)/PP(4) and PS (2)/PP(3) are shown in Appendix C. The tables consist of the ensemble mean averages, standard deviations, the maximum droplet sizes, and the minimum droplet sizes.

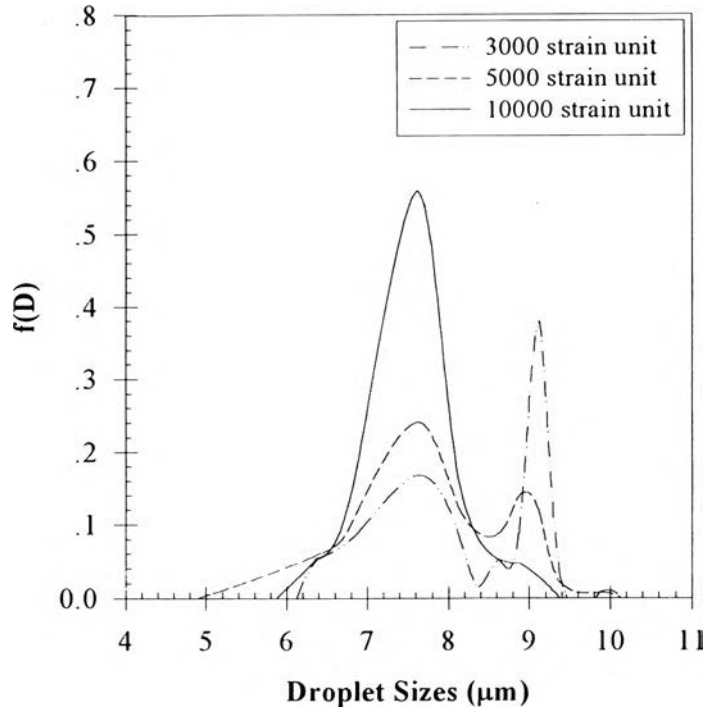

Figure 4.7 Distribution function of droplet size for PS(1)/PP(4) blends as a function of shear strain unit at shear strain rate of 10 s^{-1}.

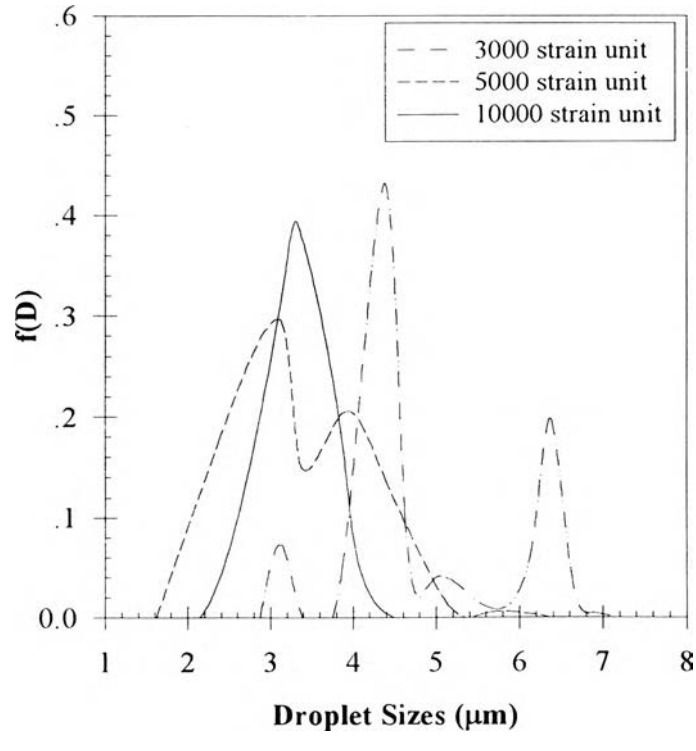

Figure 4.8 Distribution function of droplet size for PS(1)/PP(4) blends as a function of shear strain unit at shear strain rate of 100 s^{-1}.

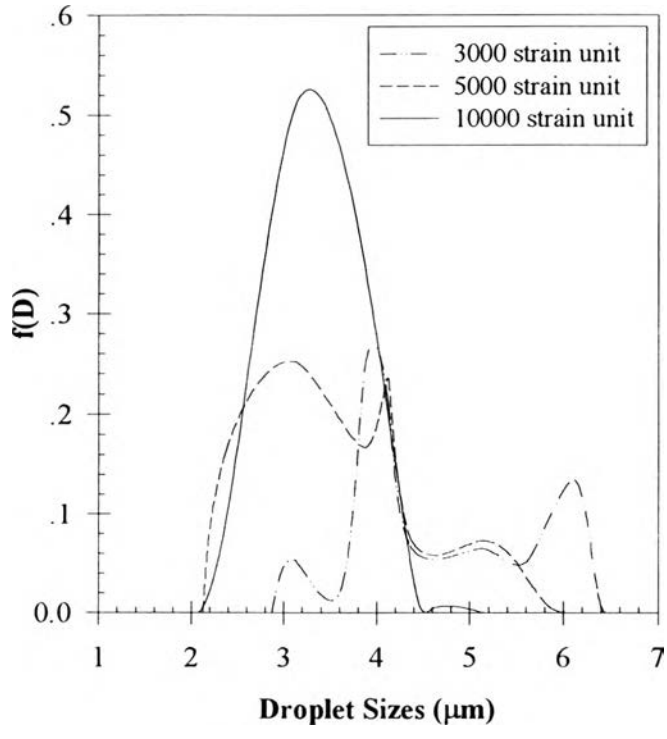

Figure 4.9 Distribution function of droplet size for PS(2)/PP(3) blends as a function of shear strain unit at shear strain rate of 10 s^{-1}.

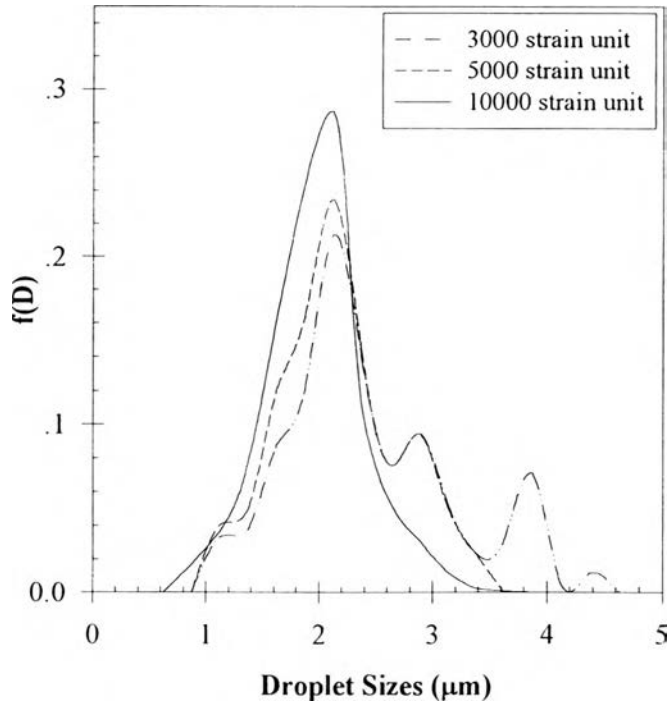

Figure 4.10 Distribution function of droplet size for PS(2)/PP(3) blends as a function of shear strain unit at shear strain rate of 100 s^{-1}.

4.3 Effect of Shear Strain Rate

4.3.1 Droplet Size

The effect of shear strain rate on equilibrium droplet size of dispersed phase was investigated at the shear strain rates of 10 to 200 s^{-1}, at 220 ^{0}C and is shown in Figure 4.11. The equilibrium droplet size decreases with increasing shear rate, so only drop breakup mechanism occurs in our experiment. Because of the higher shear viscosity ratio at any given shear rates, the PS(1)/PP(4) blends provide larger droplet sizes of the dispersed phase.

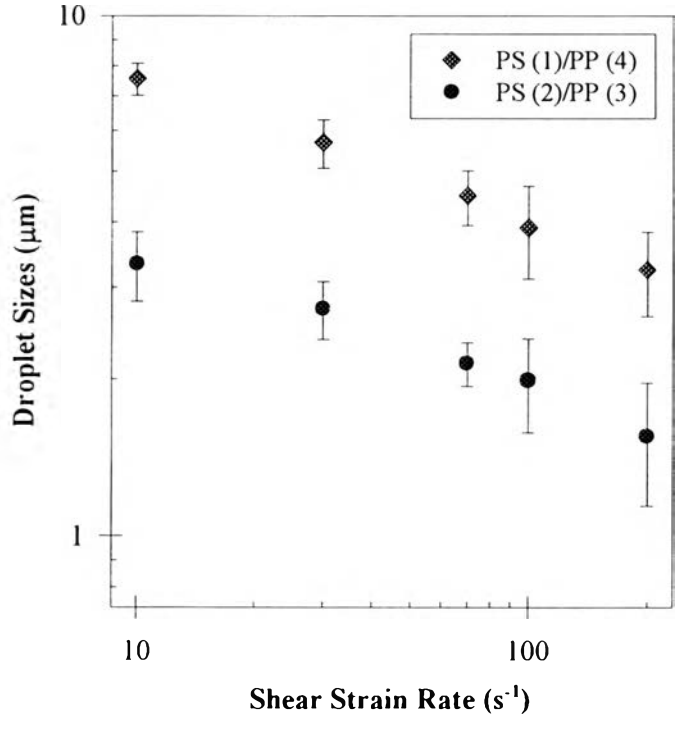

Figure 4.11 The equilibrium droplet size as a function of shear strain rate of PS(1)/PP(4) and PS(2)/PP(3) blends at 220 ^{0}C.

In this experiment, droplet size decreases proportional to the shear strain rate with the power law exponent of –0.3. The power law exponent obtained from Taylor's theory and Wu's correlation (eq. 1.3 and 1.4) is exactly –1. In the case of Taylor's theory, the theory was derived for a Newtonian system without the elastic effect. So the decrease in equilibrium droplet size as a function of shear strain rate of our blends is less than that of the Taylor's theory due to the elastic effect.

In the case of Wu's correlation, the correlation was obtained from polymer blends, but the experiment was carried out in an extruder. The flow generated from this machine is of non-uniform shear strain rates: a combination between elongational flow and shear flow. The elongational flow can break the drop more effective than the shear flow. So the decrease in equilibrium droplet size from Wu's correlation is much higher than that obtained from our experiment.

The micrographs obtained from the optical microscope for the effect of shear strain rate are shown in Appendix B. The summarized data of the effect of shear strain rates on the equilibrium droplet size are shown in Appendix C.

4.3.2 Distribution Function of Droplet Size

To observe the progress of the droplet size as a function of shear strain rate, the plots of distribution functions at the shear rate of 10, 70, and 200 s^{-1} are shown in Figures 4.12 and 4.13. The plots show that the distributions shift to a smaller droplet size when shear strain rate increases.

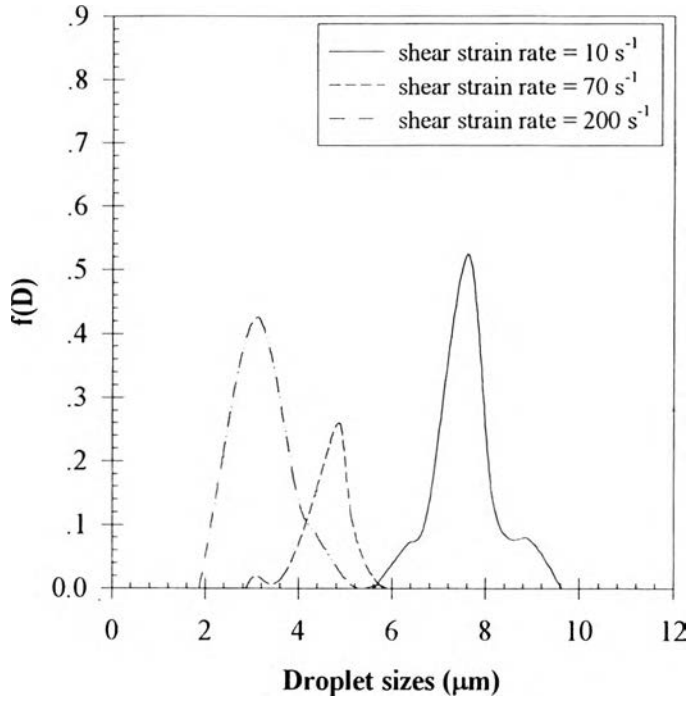

Figure 4.12 Distribution function of droplet size of PS(1)/PP(4) as a function of shear strain rate at 220 ^{0}C.

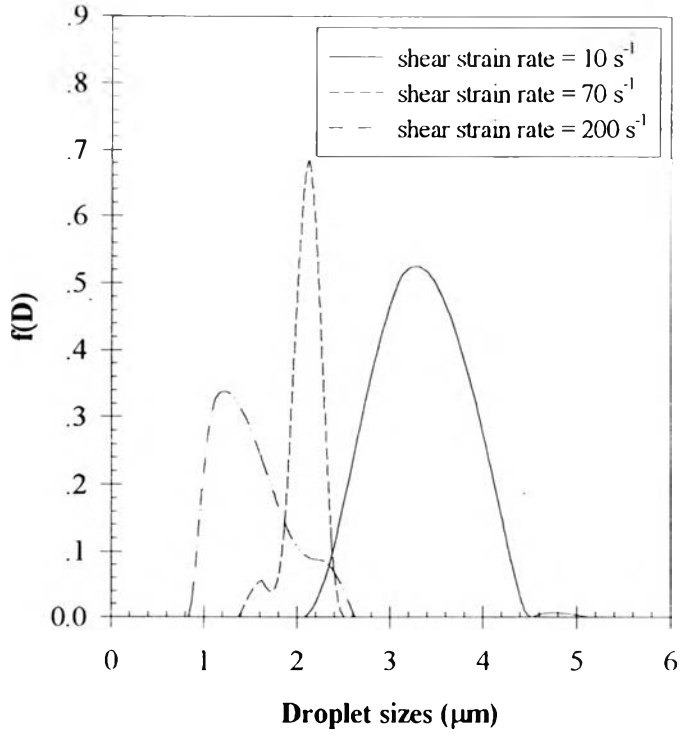

Figure 4.13 Distribution function of droplet size of PS(1)/PP(4) as a function of shear strain rate at 220 ^{0}C.

4.4 The Correlation between Viscoelastic Properties and Morphology of Immiscible Polymer Blends

The morphology of immiscible blend depends on rheological properties, thermodynamic properties, processing conditions, and composition. The dimensionless capillary number (Ca) has been used to determine the ratio of viscous force ($\eta_m\dot{\gamma}$) over interfacial force (Γ / D). The other important dimensionless parameters, such as viscosity ratio (η_d/η_m) and the first normal stress difference ratio ($N_{1,d}/N_{1,m}$) will be used to correlate with Ca.

4.4.1 The Viscosity Ratio and the First Normal Stress Difference Ratio of the Blends

As mentioned in section 4.2.1, the morphology was developed rapidly in the initial stage of shearing and the final rheological properties do not influence the equilibrium droplet size, so the shear viscosities and the first normal stress difference used in calculating the shear viscosity ratios and the first normal stress difference ratios were obtained from the rheological properties at pre-shearing. The equilibrium droplet size at the shear strain unit of 5000 were chosen to minimize the polymer degradation that occurs after shearing for a long time, and to obtain the equilibrium droplet size on the ensemble mean basis, nearly identical to the statistical equilibrium droplet size at the shear strain unit of 20000. All of the shear viscosities ratios and the first normal stress difference ratios obtained from polymer matching between PS and PP were categorized into 4 groups depending on the shear viscosity ratio. Tables 4.4 (a-d) show the rheological data of PP and PS for shear viscosity ratios, the first normal stress difference ratios, shear rate, interfacial tension, and equilibrium droplet sizes at the shear strain unit of 5000 at 220 ^{0}C.

Table 4.4 (a) The first normal stress difference ratio of PS/PP blends at the shear viscosity ratio of 0.5

Polymer pairs	γ (s^{-1})	Γ^* (dyn/cm)	η_r	$N_{1,r}$	Equilibrium droplet sizes (μm)
PS(3)/PP(3)	30	4.78	0.53	0.32	3.21 ± 0.65
PS(2)/PP(3)	10	4.78	0.48	0.35	5.16 ± 1.44
PS(2)/PP(3)	20	4.78	0.47	0.40	3.97 ± 1.72
PS(3)/PP(3)	50	4.78	0.53	0.47	3.48 ± 0.88
PS(2)/PP(1)	50	4.78	0.53	0.51	4.07 ± 1.11

* Appendix D

Table 4.4 (b) The first normal stress difference ratio of PS/PP blends at the shear viscosity ratio of 1

Polymer pairs	γ (s^{-1})	Γ^* (dyn/cm)	η_r	$N_{1,r}$	Equilibrium droplet sizes (μm)
PS(3)/PP(2)	30	4.78	0.79	0.35	1.43 ± 0.30
PS(2)/PP(2)	20	4.78	0.82	0.41	1.60 ± 0.48
PS(2)/PP(2)	30	4.78	1.04	0.53	1.70 ± 0.41
PS(3)/PP(3)	100	4.78	1.14	0.69	1.11 ± 0.36
PS(3)/PP(4)	50	4.78	1.05	0.92	1.37 ± 0.38
PS(2)/PP(4)	50	4.78	0.98	1.12	1.66 ± 0.42

Table 4.4 (c) The first normal stress difference ratio of PS/PP blends at the shear viscosity ratio of 2

Polymer pairs	γ (s^{-1})	Γ^* (dyn/cm)	η_r	$N_{1,r}$	Equilibrium droplet sizes (μm)
PS(2)/PP(2)	50	4.78	1.68	0.94	3.89 ± 0.89
PS(3)/PP(4)	100	4.78	1.95	1.16	3.87 ± 1.03
PS(1)/PP(3)	10	4.78	1.90	1.51	3.60 ± 0.92
PS(1)/PP(3)	70	4.78	2.41	1.68	3.56 ± 1.16

Table 4.4 (d) The first normal stress difference ratio of PS/PP blends at the shear viscosity ratio of 3

Polymer pairs	γ (s^{-1})	Γ^* (dyn/cm)	η_r	$N_{1,r}$	Equilibrium droplet sizes (μm)
PS(1)/PP(2)	10	4.78	2.53	1.40	3.40 ± 0.93
PS(1)/PP(3)	100	4.78	3.01	2.33	3.10 ± 0.74
PS(1)/PP(4)	30	4.78	3.19	3.39	4.53 ± 1.03
PS(1)/PP(4)	20	4.78	3.12	4.31	5.24 ± 1.04

The rheological properties after shearing at 5000 strain unit were calculated in order to compare with the initial properties as shown in Table 4.5.

Table 4.5 The shear viscosity ratios and the first normal stress difference ratio for pre and post shearing at 220 ^{0}C

Shear viscosity ratio	Polymer pairs	η_r		$N_{1,r}$	
		Pre-shearing	Post-shearing	Pre-shearing	Post-shearing
0.5	PS(3)/PP(3)	0.53	0.51	0.34	0.32
	PS(2)/PP(3)	0.48	0.52	0.37	0.35
	PS(2)/PP(3)	0.47	0.51	0.40	0.41
	PS(3)/PP(3)	0.53	0.54	0.49	0.47
	PS(2)/PP(1)	0.53	0.50	0.55	0.51
1	PS(3)/PP(2)	0.79	0.95	0.35	0.45
	PS(2)/PP(2)	0.82	1.01	0.41	0.46
	PS(2)/PP(2)	1.04	1.16	0.53	0.62
	PS(3)/PP(3)	1.14	1.16	0.69	0.74
	PS(3)/PP(4)	1.05	1.03	0.92	0.80
	PS(2)/PP(4)	0.98	1.16	1.12	1.01
2	PS(2)/PP(2)	1.68	1.91	0.94	0.88
	PS(3)/PP(4)	1.95	1.95	1.16	1.16
	PS(1)/PP(3)	1.90	1.97	1.51	2.48
	PS(1)/PP(3)	2.41	1.96	1.68	3.41
3	PS(1)/PP(2)	2.53	3.01	1.40	2.33
	PS(1)/PP(3)	3.01	3.06	2.33	3.47
	PS(1)/PP(4)	3.19	2.97	3.39	4.99
	PS(1)/PP(4)	3.12	2.97	4.31	5.17

4.4.2 The Capillary Number (Ca) and the First Normal Stress Difference Ratio ($N_{1,r}$) Correlation

The correlation between the capillary number and the first normal stress difference ratio at pre-shearing and post-shearing are shown in Figures 4.14 and 4.15 respectively.

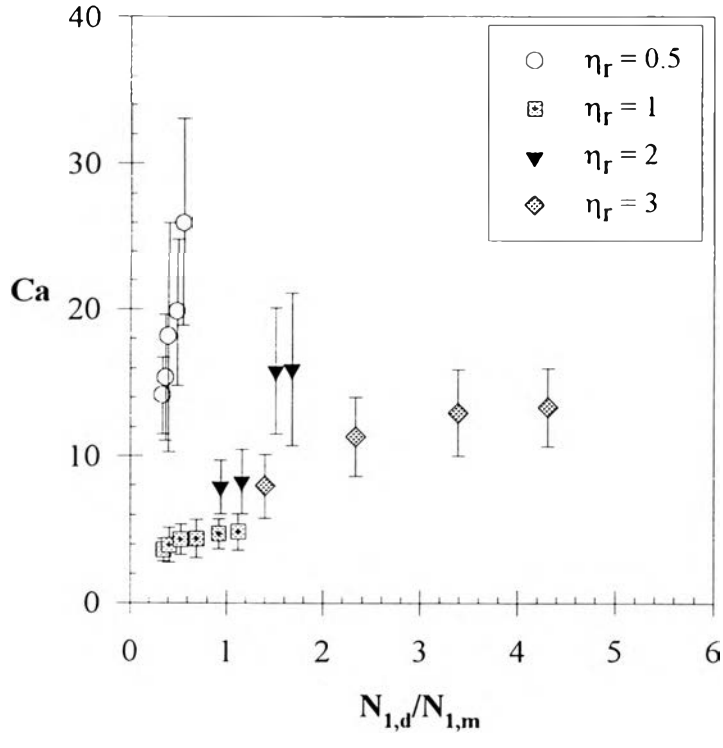

Figure 4.14 The correlation between a capillary number (Ca) and the first normal stress difference ratio ($N_{1,d}/N_{1,m}$) with various viscosity ratios at pre-shearing and at 220 ^{0}C.

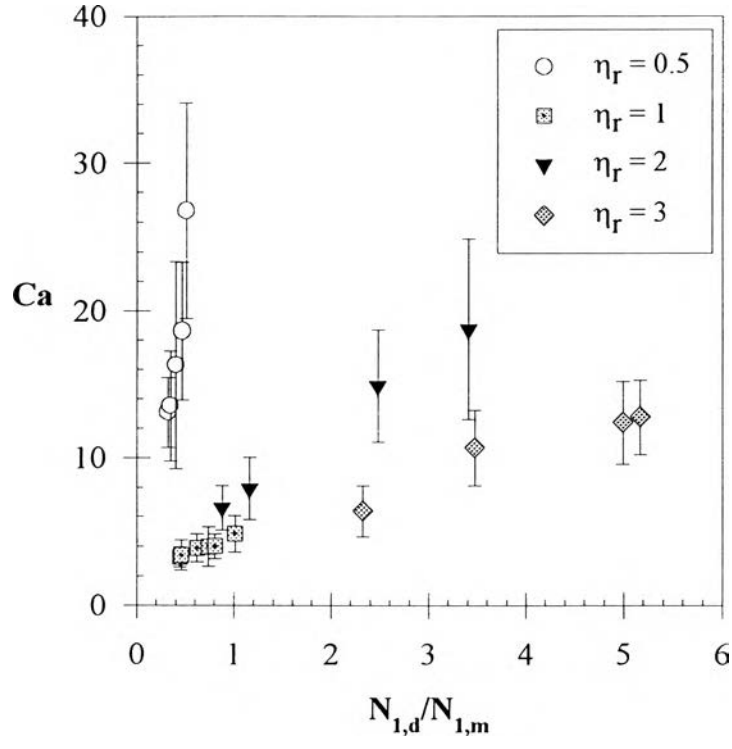

Figure 4.15 The correlation between a capillary number (Ca) and the first normal stress difference ratio ($N_{1,d}/N_{1,m}$) at various shear viscosity ratios after shearing for 5000 strain unit and at 220 ^{0}C.

There is a correlation between Ca and $N_{1,r}$ (= $N_{1,d}/N_{1,m}$) and these two graphs show qualitatively the same result. Ca increases with increasing $N_{1,r}$, meaning that the viscous force required to break the drop increases when the elasticity of drop is very large. The results are consistent as the results of other researchers (Varanasi *et al.*, 1994; Mighri *et al.*, 1998). However, most of them studied the correlation between the *critical* capillary number ($Ca_c = \frac{\eta_m \dot{\gamma}_c}{\Gamma / D}$) and the elasticity effect whereas our experiment studies the correlation between equilibrium Ca and $N_{1,r}$ of polymer melt blends. The data used in calculating Ca are tabulated in Appendix E.

Ca calculated from Taylor's theory at any shear viscosity ratio is shown in Table 4.6. The result shows that Ca from Taylor's theory ,based on the Newtonian system when both $N_{1,d}$ and $N_{1,m}$ are equal to zero, is

lower than Ca from this experiment at any given shear viscosity ratio. So our results confirm that the elasticity of drop enhances the resistance for the drop deformation in viscoelastic systems.

Table 4.6 Ca calculated from Taylor's theory at various shear viscosity ratios

Shear viscosity ratio	$Ca = \frac{4(\eta_r + 1)}{\left(\frac{19}{4}\eta_r + 4\right)}$
0.5	0.94
1	0.91
2	0.89
3	0.88

Moreover, Figure 4.14 and 4.15 show Ca obtained from the results are found to be higher for a lower shear viscosity ratio at any given $N_{1,r}$. This can be explained from the definition of Ca, which is defined as the viscous force in the matrix phase over the interfacial force in the dispersed phase. When the matrix viscosity increases (decreasing viscosity ratio), Ca would be increased at the same elasticity ratio. The results are in qualitative agreement with that of calculated from Taylor's theory. The exception to the above result occurs when the shear viscosity ratio is equal to 1. We do not understand the reason for this.